Renewable Energy 113 (2017) 1019–1032

Contents lists available at ScienceDirect

Renewable Energy

journal homepage: www.elsevier.com/locate/renene

System design and operation for integrating variable renewable energy resources through a comprehensive characterization framework

Madeleine McPherson [a, *], L.D. Danny Harvey [b], Bryan Karney [a]

[a] Department of Civil Engineering, University of Toronto, 35 St. George Street, Toronto, ON, M5S 1A4, Canada
[b] Department of Geography, University of Toronto, 100 St. George Street, Toronto, ON, M5S 3G3, Canada

ARTICLE INFO

Article history:
Received 21 December 2016
Received in revised form
4 June 2017
Accepted 19 June 2017
Available online 20 June 2017

Keywords:
Variable renewable energy integration
VRE characterization
VRE flexibility resources
Electricity system dispatch model

ABSTRACT

The name itself – VRE for variable renewable energy – encapsulates the essential challenge: these energy sources are attractive precisely because they are renewable and yet problematic because they are variable. Thus, integrating large penetrations of VRE resources such as wind and solar into the electricity grid will necessitate flexible technologies and strategies. This paper establishes characterization metrics of both individual VRE resources and aggregated VRE resource sets with the goal of quantifying the integration requirements of various typologies. Integration requirements over multiple time scales are considered including hourly, weekly - seasonal, and inter-annual flexibility, as well as transmission expansion to connect neighboring wind and solar sources, and demand response mechanisms. The respective integration requirements are quantified through storage and demand response utilization rates, VRE curtailment rates, non-VRE ramping requirements, system costs, and GHG emissions. The results from VRE resources across South America clearly quantify the impact that integrating different VRE regimes has on the electricity system design and operation: not surprisingly integrating VREs on a grid with low non-VRE flexibility incurs the largest integration requirements, while smoothing net VRE production with out-of-phase resources is an effective integration strategy.

© 2017 Elsevier Ltd. All rights reserved.

1. Introduction

Among other things, the transition to a sustainable energy system depends on harnessing renewable resources for electricity generation. Aside from hydro resources, the two most important renewable resources, wind and solar, are variable in nature. The implications of achieving large variable renewable energy (VRE) penetration in the electricity grid are not fully quantified, nor the range of balancing options fully explored. In part, the particular characteristics of a VRE regime impacts the specific combination of flexibility resources that are required for its integration. As such, characterizing VRE regimes according to their integration requirements is a critical step in the integration process, and is the primary subject of the current paper.

As a preliminary example, consider that wind resources are often characterized using the Weibull distribution, which describes windspeed distributions according to their annual mean windspeed and shape factor. While straightforward, the Weibull distribution is not a holistic representation [19,23,33]. Alternative characterizations provide a more nuanced view of VRE variability: relationship between the mean and median wind power density (WPD), coefficient of variance, robust coefficient of variance, interquartile range, inter-annual variation, consecutive hours above or below a set WPD threshold (episode length), WPD availability above a given threshold, and anticoincidence with the surrounding grid cells [7,11,14,19]. System-level analyses include the effective load carrying capability [20], the effect of temporally shifting a resource [29] and the net load curve variability [22]. The current work seeks to closely tie wind characteristics to an overall system or VRE characterization for the grid.

In parallel to studies on specific resources, other studies have explored the impact of large-scale VRE integration at a range of system scales. For example, a techno-economic analysis quantified the impact of replacing conventional technologies with optimized hydrogen-based systems in renewable-based stand-alone power

* Corresponding author.
E-mail addresses: madeleine.mcpherson@mail.utoronto.ca (M. McPherson), harvey@geog.utoronto.ca (L.D.D. Harvey), karney@ecf.utoronto.ca (B. Karney).

http://dx.doi.org/10.1016/j.renene.2017.06.071
0960-1481/© 2017 Elsevier Ltd. All rights reserved.

systems [50]. Distribution scale analyses have studied the impacts of high VRE penetration on distribution networks in Lisbon and Helsinki [35], and the Davarzan area in Iran [48]. Transmission scale analyses have quantified the integration of high wind, solar PV, and/or wave power in Austria [8], Central Queensland [44], and Vancouver Island [32], have identified the optimal mixtures of VREs to avoid excess electricity production in Denmark [27], and have analyzed the desalination plants as a deferrable load in Saudi Arabia [1]. Further studies have analyzed the impact of VRE integration on specific non-VRE generation assets such as hydropower resources and their associated river flow patterns [24], or thermal power plant operational cycles [17]. Others have studied the impacts of integrating renewable energy shares outlined in national policies in North-West Europe [12], or the impact of storage size and efficiency on achieving 100% renewable systems [49]. Finally, a suite of studies has quantified VRE integration economic costs through metrics such as increased need for balancing services and flexible operation of thermal plants, and reduced utilization of capital embodied in thermal plants [21].

This paper aims to bridge the gap between VRE characterization analyses and integration requirements by presenting a new VRE resource characterization framework that maps VRE characterizations to specific balancing strategies. VRE resources are characterized according to their hourly, weekly, seasonal, and inter-annual temporal variability, as well as their geographic coincidence factor, inter-resource coincidence factor, and correlation with the demand profile. These metrics map to specific balancing strategies: storage technologies with daily or seasonal reservoir capacity, VRE curtailment, increasing the non-VRE grid flexibility, interconnecting geographically dispersed resources and VRE types, and demand response (DR) mechanisms. The proposed characterization framework enables optimization of integration strategies for a given suite of VRE projects. Although applied to a specific geographical area, the methodology illustrated is general in scope.

The remainder of this paper is organized as follows: Section 2 first describes the VRE resource data that were used in this analysis, while Section 3 details the six developed VRE characterizations. Section 4 then quantifies the impacts of integrating VRE resource regimes with distinct typologies in a production cost model. Finally, Section 5 discusses the overall results and Section 6 presents our conclusions.

2. VRE resource data

Multi-decadal, continentally-scaled wind and solar PV generation timeseries with hourly temporal resolution were produced using the Global Renewable Energy Timeseries and Analysis (GRETA) tool [31]. GRETA applies the Boland-Ridley-Lauret [6] and Perez [38] models to NASA's MERRA radiation fluxes dataset to calculate hourly solar PV generation, and the Archer and Jacobson Least Squares Fit [2] methodology to the MERRA atmospheric reanalysis dataset to calculate hourly wind generation. The MERRA reanalysis dataset, developed by NASA [26,40], aggregates weather observations from satellite and surface stations, aircrafts, and balloons through a Numerical Weather Prediction (NWP) model [7]. Reanalysis datasets offer key advantages for creating the VRE resource estimates employed in this analysis, including global coverage and long data collection periods [5], and consistent extrapolation methodology [7,19]. MERRA provides the variables required to compute wind and solar generation potential on a global ½° by 2/3° latitude-longitude grid with hourly resolution from early 1979 to within 2 months of the present. GRETA has the same spatial and temporal resolution. The calculations assume a 100 m wind turbine hub height and use the Vestas-112-3.0 turbine power curve for wind electricity, and assume fixed tilt solar panels with an elevation angle equal to the location's latitude and use the First Solar FS395 power curve for solar electricity.

To illustrate the methodology, this analysis explores the VRE resource regimes available on the South American continent. South America is chosen because it has high solar resource availability in the Atacama Desert, Caribbean coast, and eastern Brazil, as well as excellent wind resources in Patagonia, Paraguay, and Bolivia. Although country-specific VRE characterizations analyses have been conducted in Brazil (Schmidt, Cancella, & Pereira Jr., 2016) and the Lerma Valley in Argentina [39], the entire South American continent, including the regions listed above, has not yet been considered, to the author's knowledge. The characterization analysis is limited to 'utility-quality' VRE regimes, defined as locations with an average annual windspeed greater than 6.4 m/s, or an average annual solar irradiance greater than 5.7 kWh/m^2/day. Fig. 1 highlights the grid cells that meet this criterion, using data from the National Renewable Energy Laboratory [16,34]. The characterization analysis was performed using more than 650 utility-quality cells over 35 years, resulting in almost 200 million data points. The following sections detail the characterization framework developed to probe such a data set by quantifying balancing requirements for distinct VRE regimes. The goal is to identify and highlight the most effective balancing strategies.

3. VRE regime characterization

A VRE regime's temporal variability, geographic correlations, and net load curve characteristics necessitate different integration technologies or strategies. Table 1 maps each VRE characterization metric with the appropriate integration strategy. The suggested proposal is advanced as a candidate balancing strategy, a hypothesis which is subsequently tested using a unit commitment model.

Each of the following metrics is first formulated and then applied over 650 South American grid points according to 35 years (1979–2013) of historical meteorological data. For simplicity of notation, sums over the whole data set are reduced from $\sum_{1979}^{2013}$ to the form $\sum_{n}$. A number of metrics are used to more comprehensively characterized each VRE resource.

3.1. Hourly variability

Ramp events are calculated by the rate of change in wind speed

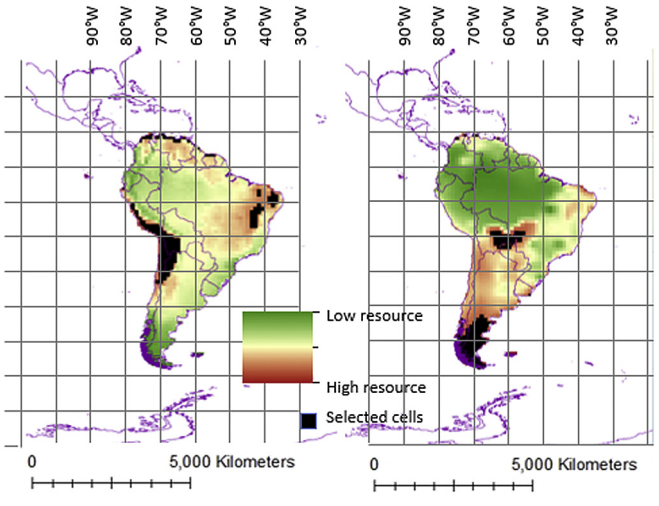

Fig. 1. Utility-quality solar PV (left) and wind (right) grid cells in South America that were selected for analysis.

Table 1
Resource variability metrics mapped to integration strategies.

Characterization metric	Metric formulation	Corresponding integration strategy
Variability over hourly timescale	Hourly ramp events frequency and magnitude (Eq. (1))	Storage technologies with daily reservoir capacity, VRE curtailment, and increasing the non-VRE grid flexibility factor
Variability over weekly-seasonal timescale	Relative frequency distribution curve (Eq. (2))	Storage technologies with annual reservoir capacity, and increasing the system's firm capacity
Inter-annual variability	Annual average capacity factor distribution (Eq. (3))	Long-term storage technologies, sector integration, and backup generation
Correlation with demand profile	Average resource within low or high demand portions of the day (Eq. (4))	Demand response initiatives
Geographic coincidence factor	Coincidence of an increasingly large geographic area (Eq. (5))	Transmission capacity expansion with neighboring areas
Inter-resource coincidence factor	Correlation between wind and solar resources (Eq. (6))	The respective share of wind versus solar resources

magnitude, as measured in meters per second, between consecutive hours, thus resulting in units of $[m/s]/h$. We define the mean absolute ramp rate (E_{MARV}), between consecutive hours over the 35-year period as:

$$E_{MARV} = \frac{\sum|v_i - v_{i-1}|}{n-1} \quad (1)$$

where v_i refers to the wind speed in the hour i, and n is the number of hours over the 35-year sequence. The mean absolute ramp rate for each grid point was calculated, then three categories are defined at the 33 and 67 percentile values, such that each category contains one third of the grid points. The cut-offs for the mean absolute ramp categories were calculated to be 0.41 m/s per hour and 0.45 m/s per hour for the wind resource, and 76 W/m^2 and 83 W/m^2 per hour for the solar resource. Fig. 2 shows an example of a low, moderate and high hourly variability wind resource over one year.

The correlation between increasing average windspeed and the mean absolute ramp rate is weak (correlation, $r = 0.126$). There is a wider range in ramp rates among grid points with a lower average windspeeds, as shown in Fig. 3.

The same trend is observed for the solar resource: lower average irradiance sites tend to have lower E_{MARV} (correlation, $r = 0.848$). Like wind, lower irradiance sites have a larger E_{MARV} range, as shown in Fig. 4.

3.2. Weekly-seasonal variability

Weekly-seasonal variability is quantified by a regime's relative frequency. The maximum relative frequency (E_{MRF}) formulation for a wind resource is:

$$E_{MRF} = \frac{\max_{0<i\leq 23} y_i}{n} \quad (2)$$

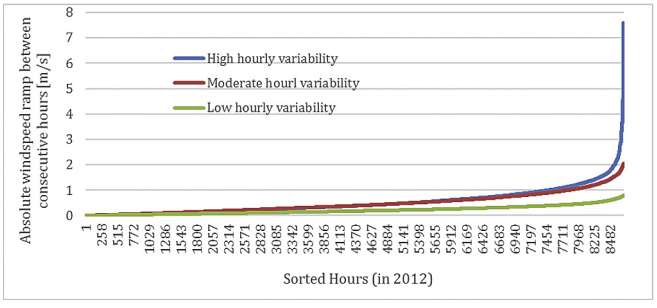

Fig. 2. Ramp rates for a sample year (2012) for grid points with low, moderate, and high hourly variability.

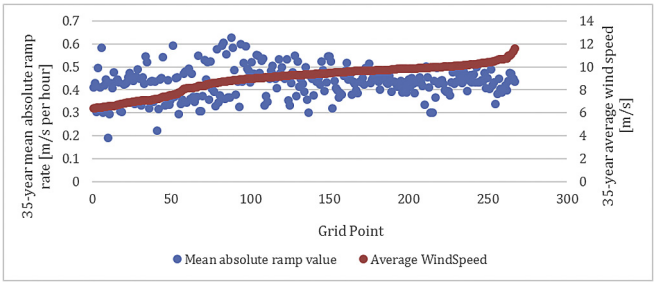

Fig. 3. Mean absolute ramp rate and average windspeeds.

where y_i is the number of samples within bin i, with bins spanning the range from 0 to 23 m/s in 1 m/s intervals, and n represents the total number of samples (hours) over the 35-year period. Resources with high maximum relative frequency are consistently found within a specific resource bin (not necessarily the largest bin) and have a narrow relative frequency distribution, requiring less balancing for integration. Conversely, regimes with a small maximum relative frequency and a broad relative frequency distribution require more non-VRE flexibility for integration. Examples of wind regimes with low, medium, and high seasonal variability are shown in Fig. 5.

The maximum relative frequency is correlated with the average windspeed: lower average windspeed grid points tend to have a higher maximum relative frequency and vice versa (Fig. 6). This is intuitive: regimes with low average windspeed are consistently weak, resulting in a higher maximum relative frequency, while high average windspeed grid points have a larger windspeed spread and lower maximum frequencies. From year to year the relative frequency distribution varies more for regimes with higher overall maximum relative frequency.

In general, solar resources have a wider relative frequency

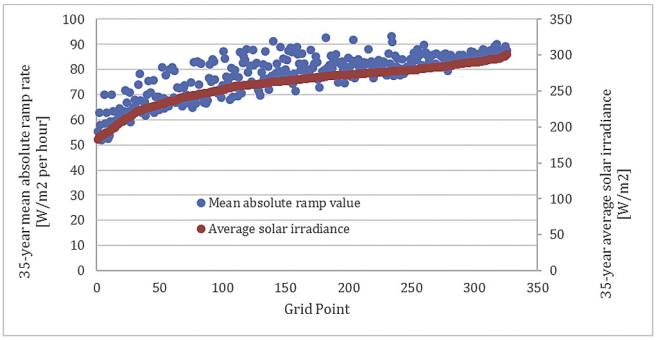

Fig. 4. Mean absolute ramp rate and average solar irradiance.

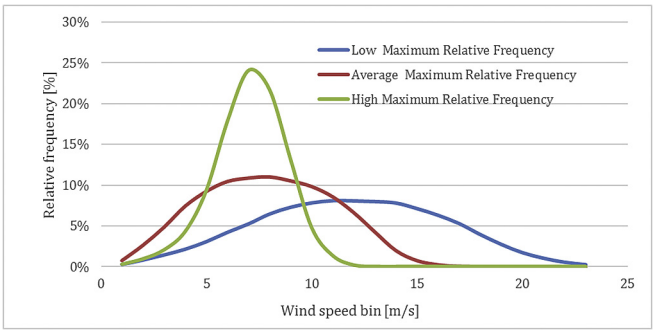

Fig. 5. Relative frequency of windspeeds with low, average, and high seasonal variability.

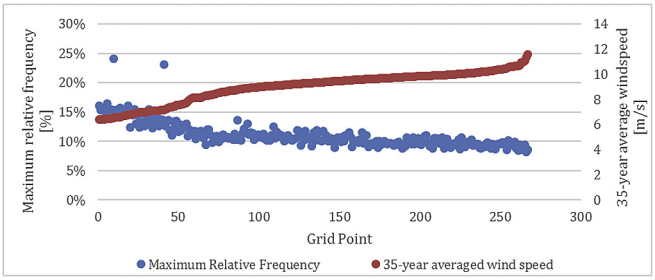

Fig. 6. Relationship between the maximum relative frequency and average windspeed.

distribution and smaller maximum relative frequency than wind resources: solar points clearly fluctuate from zero to (near) peak levels on a daily basis. The variability among different solar resources is also narrower as shown in Fig. 7. Like wind, grid points with larger average irradiance have smaller maximum relative frequency, although to a lesser extent than wind.

3.3. Inter-annual variability

Inter-annual variability is calculated by determining the variance between the annual average resource and the 35-year average resource. The inter-annual variance (E_{IAV}) formulation is:

$$E_{IAV} = \frac{\sum_{n=1}^{35} (y_i - \mu)^2}{35} \quad (3)$$

where y_i is the is the average resource value in year i, and μ is the 35-year average. Three inter-annual variability categories are defined with boundaries at variances of 0.12 and 0.19 $(m/s)^2$ per year for wind, and at 5.8 and 35 $(W/m^2)^2$ per year for solar; each category contains one third of the points.

The most variable wind grid point has average inter-annual variation of 10%, and a maximum annual variation of 22%; however, over 70% of points have a 35-year average inter-annual variation less than 4%. Overall, solar resources experience a smaller range in inter-annual variation than wind. The most variable solar grid point has an average inter-annual variation of 5%, less than half the respective value for the wind resource.

The inter-annual variance is closely related to the interquartile range, as shown for the wind grid points in Fig. 8. Wind grid point's interquartile range spans from 0.19 to 1.10 m/s while the variance ranges from 0.02 to 0.56 $(m/s)^2$ per year.

3.4. Correlation with demand profile

Demand response (DR) can at least partly shift the load profile to match the available VRE resource. DR's utility is informed by the correlation between the VRE resource and the demand profile. A characteristic demand profile was approximated by allocating each hour in the day to one of four demand blocks, ranging from low demand hours in block 1 to high demand hours in block 4. The approximated demand profile is built from publicly available historical Chilean demand data (including all consumer categories) from the Chilean electricity system regulator [9,10]. The DR metric is formulated by averaging the resource within each block, normalizing to the 35-year average, and summing over the four DR blocks to produce the aggregate DR metric. The DR metric (E_{DR}) formulation is calculated as follows:

$$E_{DR} = y_1 + 2y_2 + 3y_3 + 4y_4 \quad (4)$$

where y_1, …, y_4 is the average resource value (m/s or W/m^2) observed in the respective demand block 1, …, 4 (as defined by the demand profile shown in Fig. 9). For example, y_1 is the average resource value for the hours in the day which fall into demand block 1. Resources during demand block 2 carry twice as much weight as resources during demand block 1 (from a demand-matching perspective), because the average demand in block 2 is twice that in block 1, after subtracting the minimum demand; similarly for the weighting factors of 3 and 4 for resource values during demand blocks 3 and 4. Fig. 9 shows the variation with hour of day in wind speed and the demand profile, averaged over 35 years of hourly data, for two example grid points, one with a low correlation between wind and demand, and the other with a high correlation.

Fig. 10 demonstrates how the aggregated DR metric for wind varies among the grid points. Only 30% of points have a higher average windspeed in low demand hours as compared to their overall average. The DR metric variation is larger for lower average windspeed points, ranging by over 5%, compared to only 2% for points with higher average windspeeds.

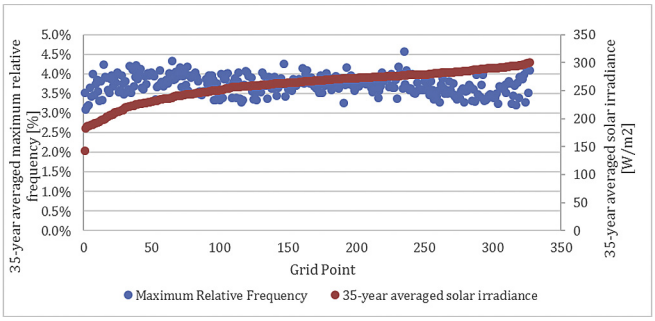

Fig. 7. Relationship between the maximum relative frequency and the average solar irradiance.

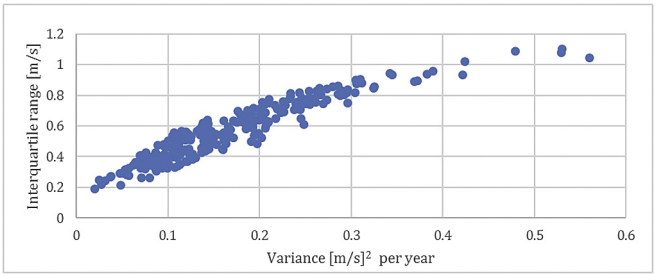

Fig. 8. Relationship between variance and interquartile range for the wind grid points.

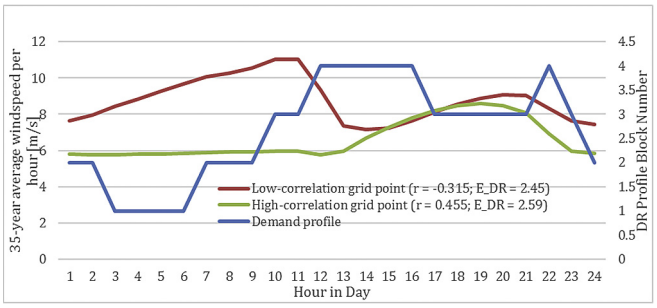

Fig. 9. The DR block number plotted against the 24-h average windspeed for well-correlated and anti-correlated wind regime; note the correlation (r) and DR metric value (E_DR) shown in the legend.

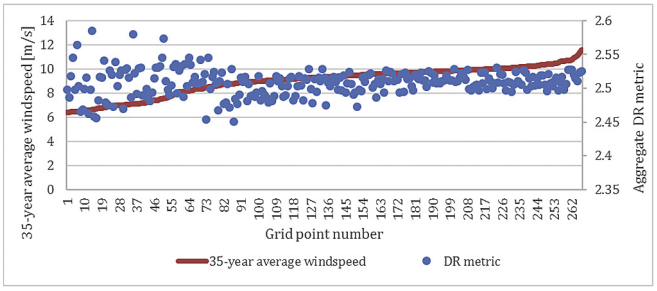

Fig. 10. Relationship between the aggregate DR metric and the 35-year average windspeed.

Predictably, all solar points have higher average irradiances in high demand hours, resulting in an average E_{DR} of 3.55 across all grid points. There is a positive correlation ($r = 0.576$) between the E_{DR} and the average irradiance: high average irradiance points have a proportionally higher irradiance in high demand hours, as compared to their low average irradiance counterpart (Fig. 11).

3.5. Geographic coincidence factor

The geographic coincidence factor measures the correlation among neighboring areas' regimes, to inform the benefit of transmission interconnection. The continuous geographic coincidence factor (E_{CF}) formulation is computed as:

$$E_{CF} = \frac{\max\limits_{1\le h\le 24}\left\{\sum_{n=1}^{N}\widehat{y_{n,h}}\right\}}{\sum_{h=1}^{24}\left(\max\limits_{1\le n\le N}\widehat{y_{n,h}}\right)} \tag{5}$$

where $\widehat{y}_{n,h}$ is the mean resource magnitude at location n, for a given hour h of each day. The following simple example, comparing well-correlated and anti-correlated wind pairs over one day, illustrates the geographic coincidence factor.

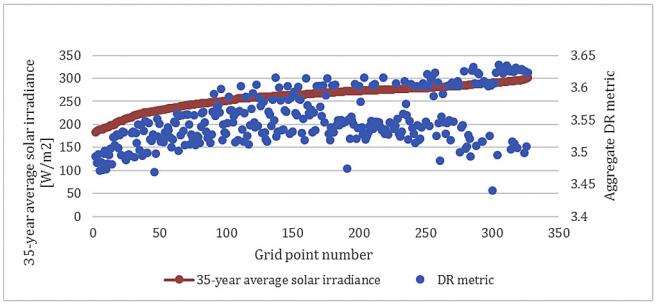

Fig. 11. Relationship between the aggregate DR metric and the 35-year average solar irradiance.

The windspeed timeseries in Fig. 12 have geographic coincidence factors of 0.13 and 0.087 for the well-correlated and anti-correlated pairs, respectively. This simple example compares only two grid points in a single day; however, practical applications calculate the geographic coincidence factor for a given set of N points using the mean resource over multiple years; thus, this simple example results in high geographic coincidence factors than more aggregated practical applications. The geographic coincidence factor is low for non-coincident sets (e.g. 0.035 for a group of 10 points in the Patagonia Group 1 set), and high for coincident sets (e.g. 0.045 for a group of 10 cells in the Bolivia Group 4 set). The geographic coincidence factor decreases for increasingly large groups of grid points; for example, the geographic coincidence factor decreases from 0.05 for two grid cells to 0.035 for 50 grid cells in an example set in Bolivia. However, the rate of change depends on the points included in the set, as shown in Fig. 13.

Wind's geographic coincidence factors changes depending on the area of the set of points under consideration: increasing cluster sizes from 2 to 50 induces a smaller change in geographic coincidence factor in Patagonia (average of −0.0104) as compared to Bolivia (average of −0.0129), as shown in Fig. 13.

Predictably, solar tends to have a higher coincidence factor than wind for the same sized set of points: wind's coincidence factor depends on the choice of specific points, whereas solar's coincidence factor depends on its location.

3.6. Inter-resource coincidence factor

The inter-resource correlation factor (E_{IRC}) informs the value of interconnecting wind and solar regimes by comparing the 35-year averaged wind and solar resource for each hour in a given day, as formulated in the following way:

$$E_{IRC} = \sum_{n=1}^{24}\chi_n \tag{6}$$

where,

$$\chi_n = \begin{cases} 1 & \psi_{n,w} = \psi_{n,s} \\ 0 & \psi_{n,w} \neq \psi_{n,s} \end{cases}$$

$$\psi_n = \begin{cases} 1 & y_n > \overline{y_n} \\ -1 & otherwise \end{cases}$$

and $\overline{y_n}$ is the daily-averaged resource, y_n refers to either $y_{n,\,w}$ (wind) or $y_{n,\,s}$ (solar) resource in hour n, and $n \in \{1,\ 2,\ 3, \ldots,\ 24\}$ hours in the day. Combinations with low aggregated inter-resource coincidence factors represent wind and solar point pairs that frequently have opposite variations (Fig. 14); these resources would benefit from interconnection. By contrast, resources with similar hourly profiles (Fig. 15), would benefit less from such interconnections.

The examples in Figs. 14 and 15 have correlations of 0.814 and −0.929, and inter-resource coincidence factors of 22 and 1 for the well correlated and anti-correlated pairs, respectively. Only 20% of wind grid points have different tendencies compared to the average than their solar counterpart in the same hour, implying a limited rationale for wind-solar interconnections within the majority of selected points in South America.

3.7. Relationships among individual characterization metrics

An aggregated view that incorporates each characterization

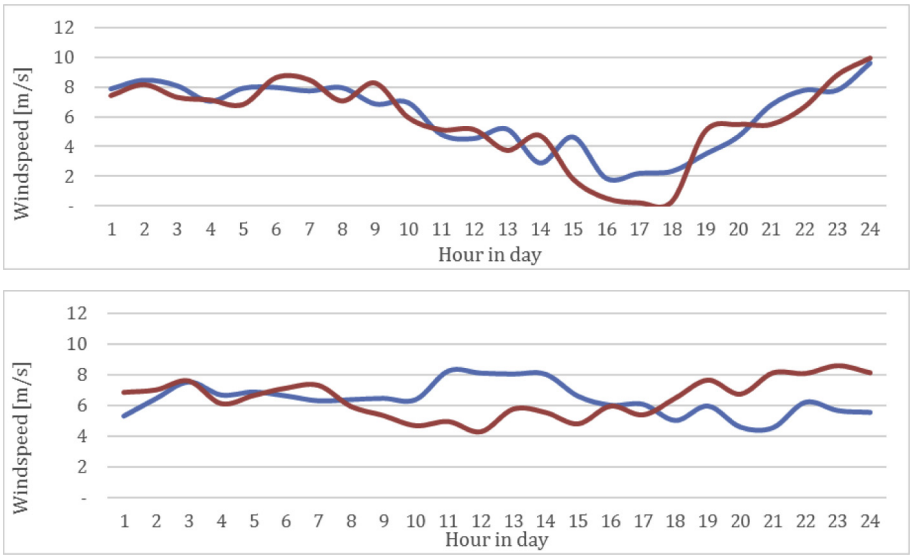

Fig. 12. Daily windspeed timeseries for a well-correlated wind pair (top), and an anti-correlated wind pair (bottom).

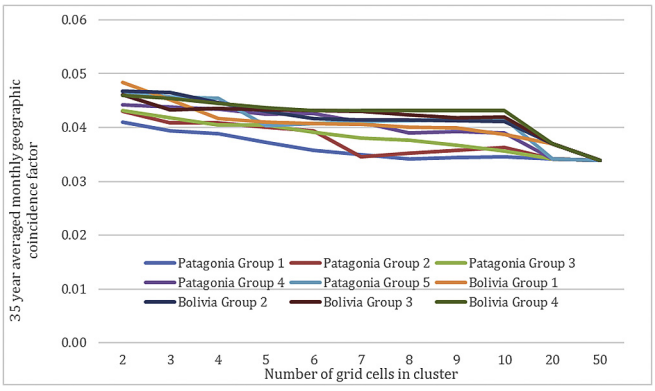

Fig. 13. Geographic coincidence factor for clusters of different sizes in Patagonia and Bolivia.

metric is desirable for understanding the relative advantage of different balancing strategies for a specific point. There is a wide range of variability characterizations for wind regimes across South America: of the 54 possible combinations of individual metrics including three hourly, weekly-seasonal and inter-annual variability categories each, as well as two DR/solar correlation categories, 51 were represented by at least one grid point. Note that for simplicity, the DR and wind-solar correlation metrics are reduced to one, since the demand profile mirrors the solar profile, as shown by the DR metric in Fig. 11. Fig. 16 shows five examples of such individual variability combinations, spanning from the least to

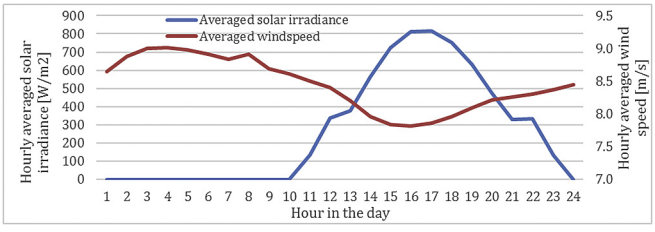

Fig. 14. 35-year averaged windspeed and solar irradiance for two anti-correlated nearby sites.

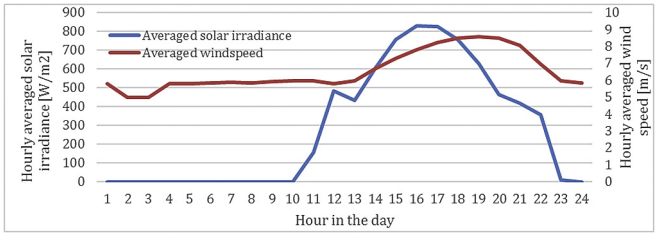

Fig. 15. 35-year averaged windspeed and solar irradiance for two well-correlated nearby sites.

most intensive integration requirements.

The 'low-variability' cumulative category (representing 16 grid points) scores one in the four individual variability categories, while the 'high-variability' cumulative category (representing 4 grid points) scores two or three in the four individual variability categories. In between, the low-medium variability represents 10

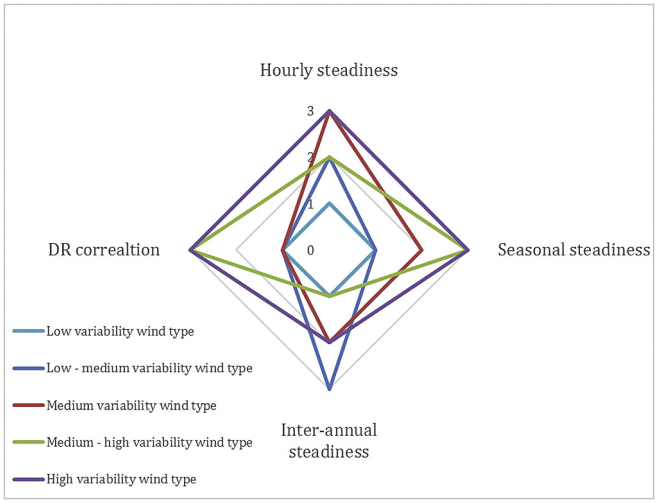

Fig. 16. Five example wind regimes categorized by differing cumulative variability requirements accounting for hourly, seasonal, and inter-annual variability, and DR/solar correlation.

Table 2
Definition of wind types according to variability characterization metrics.

Wind Type:	A	B	C	D	E	F	G	H	I
Proportion of South American cells	9%	8%	4%	6%	4%	4%	4%	4%	6%
Hourly variability	×	*	×	*	*	–	–	–	–
Weekly/seasonal variability	*	×	*	×	×	*	–	–	–
Inter-annual variability	–	×	*	*	–	×	×	*	–
Correlation with demand or solar profile	×	–	–	–	–	–	–	–	–

Table 3
Generator technology costs: total overnight cost [2012 USD/kW] from Table 8.2 of (U.S. Energy Information Administration, [46], fixed and variable O&M and fuel [2012 USD/MWh] from Table 1 of (U.S. Energy Information Administration, [47] and GHG emissions from Table A.111.2 of (Schlomer et al., [42]; Black & Vetch Holding Company, [4]).

Technology	Total overnight cost [$/kW]	Capacity factor [%]	Fixed O&M cost [$/MWh]	Variable O&M plus fuel [$/MWh]	GHG emissions [gCO2eq/kWh]
Hydro	2435	53%	4.1	6.4	24
Natural Gas (CC)	915	87%	1.7	49.1	490
Natural Gas (simple)	971	30%	2.8	82.0	490
Biomass	3919	83%	14.5	39.5	230
Wind (onshore)	2205	35%	13.0	0	11
Solar PV (utility)	3564	25%	11.4	0	48

Table 4
Generator operating constraints by technology.

Generator Type	Minimum Load [%] [4]	Cold Start [hours] [37]	Spinning Ramp Rate [%/min] [4]	Minimum off time [hours] [41]	Start-up cost [$/MW] [41][a]	Operating coefficient[c] [% of generation]
Natural Gas (simple)	50%	0.4	8.3	0	26	42%
Natural Gas (CC)	50%	3.5	5	2	66	33%
Coal/Biomass[b]	40%	3	2	8	54	33%

[a] Euros were converted to US dollars with the average 2015 EUR/USD exchange rate of 1.11
[b] Assuming coal to biomass conversion
[c] Describes the flexibility associated with each generation category

points, medium variability represents 17 points, and medium-high variability represents 23 points. The nine most prevalent cumulative categories represent approximately half of the selected South American wind grid points, shown in Table 2.

In Table 2, the symbol '×' is used to represent high balancing requirements, whereas '*' represents moderate balancing requirements, and '-' represents low balancing requirements. Wind types A and B are the most and prevalent and demanding because both require a high level of two integration strategies: high hourly variability and anti-correlation with demand or high weekly-seasonal and inter-annual variability, respectively. Wind type A is the only prevalent category that includes deployment of demand response or interconnection with solar sites as an effective balancing strategy, as expected by the relatively small number of grid points that were negatively correlated with the demand or solar profile. Conversely, wind types C-G require a high level of only one balancing strategy, and wind types H-I are the least demanding types to integrate, since they do not require a high level of any balancing strategy.

There is a strong correlation between weekly-seasonal variability and hourly variability, and between weekly/seasonal variability and inter-annual variability. Compared to wind, solar resources are more variable hourly, but less variable inter-annually. Solar resources also correlate much more with demand, decreasing the incentive for demand response initiatives. Solar has a much higher coincidence factor for the same group of points, decreasing the utility of transmission interconnection.

4. Modelling VRE typologies to quantify integration requirements

A unit commitment (UC) model is developed to quantify the balancing requirements associated with integrating different VRE typologies. The UC model minimizes the system costs over a defined optimization period, while abiding by a list of operational constraints, including: system-wide load-power balance; power limits, ramping limits, and minimum up/downs (generator, storage, and DR assets), energy limits (storage assets only), daily utilization balance (DR assets only). The UC algorithm is built on the minpower repository [18], with several modifications to include representations of demand response and storage assets, and differing integration system parameterizations. Storage technology operation is limited by additional constraints, including either pumping or generating in a given hour, and minimum and maximum energy storage constraints (e.g. the reservoir level in the case of a pumped hydro storage unit). Demand response is constrained by absolute

Table 5
Storage technology cost data [28]-Table 12.

Technology	Power Capital Cost [$/kW]	Energy Capital Cost [$/kWh]	Cycle Efficiency [%]
Pumped hydro storage	3000	12	80%
Hydrogen fuel cell	2300	15	50%

Table 6
Storage technology properties ([28]; Figure 16 & Table 12).

Storage Technology	Applicable power system size range	Applicable energy capacity	Typical storage duration	Cycle Efficiency	Discharge time at power rating
Pumped hydro storage	2 GW	48 GWh	Hours-days	85%	Hours
Hydrogen electrolysis and storage	50 MW	36 GWh	Days-months	55%	Days

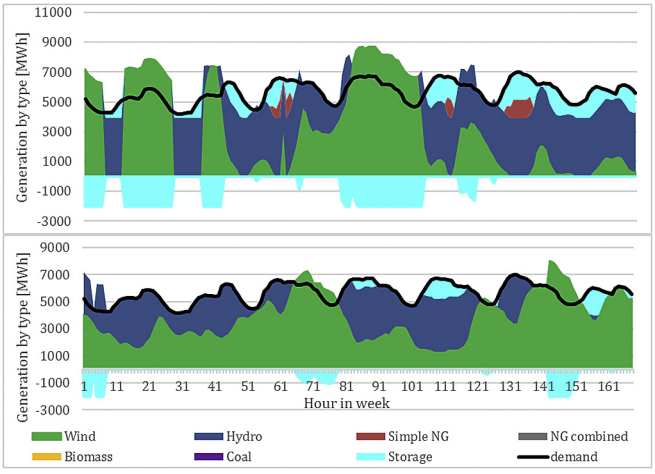

Fig. 17. Generation by technology type for an example week integrating a highly variable wind resource (top) versus a steady wind resource (bottom).

and relative (as a percentage of scheduled load) limitations on an hourly and daily basis. A series of scenarios was devised to test different integration strategies; all scenarios share the following assumptions:

- Simulation over a full year using 2012 meteorological data,
- Characteristic demand profile, with either hourly or weekly temporal resolution,
- Hydro power limitations according to historical daily flow data, published by the Chilean electricity system regulator [9,10],
- Generator cost (Table 3) and operational limitations (Table 4),
- Storage asset cost (Table 5) and characteristics (Table 6),
- VRE assets are sized such that 60% of total generation could be supplied by VRE resources prior to curtailment,
- All scenarios are normalized to have the same available VRE generation prior to curtailment.

4.1. The impact of hourly variability on integration requirements

The impact of hourly variability on integration requirements is tested through three scenarios: a baseline scenario with an average non-VRE flexibility factor grid and no VRE curtailment costs, systems with either high or low flexibility factors, and a system that incurs VRE curtailment costs. The flexibility factor represents the system's capacity to respond to variation in the net load curve and depends on the installed capacity by generation type, where each generation technology has distinct flexibility parameters (operating, ramping, and minimum downtime). The flexibility factor is discussed in more detail in Section 4.1.2. The scenarios have a 168-h optimization period, and exclude demand response and seasonal storage, which are scheduled at the daily or annual planning horizon.

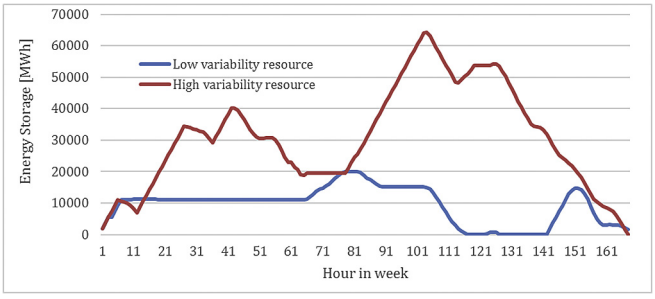

Fig. 18. Storage utilization as demonstrated by the energy stored in each hour for a system integrating a highly variable wind versus a steady wind resource.

4.1.1. Impact on a system with an average flexibility factor and no curtailment costs

The baseline scenarios assume an average non-VRE flexibility factor, represented by 55% hydro, 32% simple cycle natural gas, 8% combined cycle natural gas, 3% biomass, and 3% coal. The impact of hourly resource variability on system integration is quantified in terms of storage utilization rates, VRE curtailment rates, non-VRE ramping events, average system marginal cost, variability in marginal system cost, and GHG emissions. The system's deployment for an example week in the year is shown in Fig. 17.

Integrating a variable wind resource requires both a larger storage reservoir capacity, as shown in Fig. 18, as well as larger and more frequent storage ramping cycles compared to the steady wind resource.

Accounting for the entire year, integrating an hourly-variable wind resource results in an 82% increase in storage required, 48% increase in non-VRE or storage ramping events, and 61% increase in GHG emissions over an hourly-steady resource. Additionally, integrating a variable resource results in a 52% increase in average system marginal cost and a 118% increase in marginal cost variability (in terms of hourly spot market price). More significantly, integrating an hourly-variable resource results in a 330% increase in wind generation curtailment over an hourly-steady resource.

4.1.2. Impact on a system with a high and low flexibility factor

In addition to the VRE regime's nature, the integration requirements depend on the grid configuration characteristics. The following two scenarios explore the impact of the non-VRE flexibility on integration requirements by comparing three grid configurations, each with the same VRE regime and storage capacity but different non-VRE capacities (as shown in Fig. 19).

The system's flexibility factor is quantified by its operating, ramping, and minimum downtime flexibilities. The operating flexibility describes the flexibility of the assets dispatched in each scenario, and is a product of the operating coefficient by technology (detailed in Table 4) and the share of generation from each technology. The ramping flexibility describes the capacity of the system to adjust on an hourly basis, and is quantified by the product of the ramp rate (in MW/h per $MW_{capacity}$) by technology (detailed in Table 4) and the installed capacity by technology. The minimum downtime flexibility describes the frequency with which generation assets can be turned off and on and is quantified by the product of the minimum downtime (in hours) by technology (detailed in

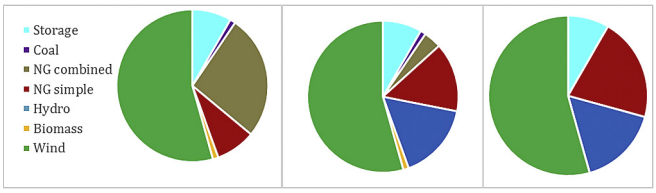

Fig. 19. Installed capacity on a system with a low (left), average (middle), and high (right) flexibility factors.

Table 4) and the installed capacity by technology. The relative flexibilities for each scenario, ranked against the inflexible system, are show in Fig. 20.

As demonstrated in an example week (Fig. 21) the combined cycle natural gas plants in the inflexible system are almost always on, even if they are at their minimum load, due to their relatively long minimum down times and expensive startup costs. This leads to a number of outcomes, including an increase of more than 300% in GHG intensity and in average system marginal cost, as well as a 125% increase in curtailment over a flexible system. Storage utilization, interestingly, is 10% higher in a flexible system, since the relatively fast spinning ramping rates of NG combined cycle plants provide ramping capacity in the inflexible system. On the other hand, utilizing the storage unit in the flexible system can avoid starting the natural gas startup and incurring the associated startup and operating costs.

4.1.3. Impact on a system that incurs curtailment costs

In a system that incurs 10 $/MWh curtailment charges with a variable wind resource, the curtailment decreases by 22%, while the storage increases by 3%, and GHG emissions increases by 39% over a system that does not charge curtailment costs.

4.2. The impact of seasonal variability on integration requirements

A seasonally variable wind regime generates well-above or below average demand for significant portions of the year, resulting in larger negative and positive net load extreme values. On the other hand, the seasonally steady regime generates more consistently throughout the year, matching average demand and resulting in smaller negative and positive net load extremes. The net load curves (electricity demand minus available VRE generation) in Figs. 22 and 23 are quantile functions, which show the number of weeks in the year for which the net load is less than the corresponding value given on the vertical axis.

The VRE curtailment resulting from negative net loads in a system integrating a seasonally variable regime can only be mitigated with seasonal storage. As a result, integrating a seasonally variable wind regime results in a 410% increase in storage asset utilization and a 211% increase in storage energy capacity compared to its seasonally steady counterpart. Fig. 23 shows the respective net load curves including storage deployment.

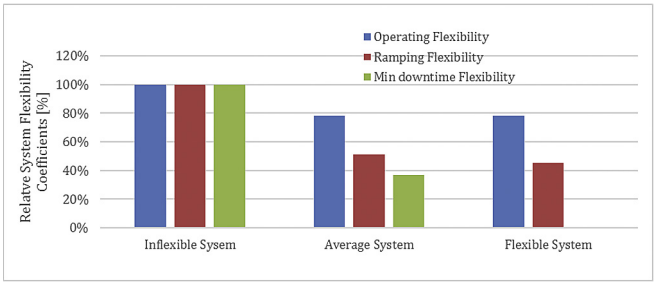

Fig. 20. System operating flexibility, ramping coefficient, and minimum downtime coefficient for three scenarios with a low, average, and high flexibility factors.

Two scenarios with averaged 52-week optimization periods were developed to test the effect of seasonal variability on integration costs; these scenarios exclude daily storage and demand response, but include seasonal storage. By deploying seasonal storage with a seasonally variable resource, the VRE curtailment is reduced to 1400 MWh or 1% of the available VRE generation, which is the result of inflexible non-VRE generators, rather than negative net load. Additionally, seasonal storage deployment reduces curtailment by over 500%, average system costs by 10%, GHG emissions by 11%, and non-VRE and storage ramping events by 9%.

Integrating a seasonally variable resource results in a 6% increase in overall system costs and GHG emissions, and 26% increase in non-VRE or storage ramping events compared to its seasonally steady counterpart. The storage unit in both scenarios has a net accumulation of 2 GW annually, which could be used in the heating or transport industries. The weekly averaged dispatch by generation type for a system with a seasonally steady versus seasonally variable resources is shown in Fig. 24.

4.3. Integrating VRE resources that correlate with the demand profile

A wind regime that is well-correlated with the demand profile will be strong during high demand hours resulting in smaller positive net loads, and weak during low demand hours resulting in smaller negative net loads. In this case, demand response, which shifts the demand profile to better align with the VRE resource, would be less attractive than its anti-correlated counterpart. Examples of the resulting net load curve for a well-correlated and anti-correlated wind regime are shown in Fig. 25.

Fig. 26 shows wind regimes that are well-correlated with the demand profile (top) and anti-correlated with the demand profile (middle). Averaged over the entire year, integrating an anti-correlated wind regime results in a 35% increase in curtailment, 24% increase in demand response utilization, 4% increase in cost, and 7% increase in marginal cost variability compared to integrating a well-correlated regime.

Storage utilization draws down the curtailment resulting from integrating an anti-correlated wind resource, as shown on the bottom portion of Fig. 26. Adding a storage asset to a system integrating a wind regime that is anti-correlated with demand reduces curtailment by 14% and demand response utilization by 12%.

4.4. The impact of geographic coincidence factors on integration requirements

Deploying two well-correlated wind regimes (with mirroring output), or two anti-correlated wind regimes (with complementing output), has a large impact on integration requirements. As shown in Fig. 27, deploying two anti-correlated wind regimes results in smaller extreme negative or positive net loads. These negative net loads result in VRE curtailment that can only be mitigated with storage utilization, but not with increased system flexibility. The smaller negative net loads in the anti-correlated set will necessitate less storage utilization to achieve the same amount of curtailment, as well as less generation from non-VRE assets due to the smaller positive net loads.

The curtailment increases from 5 GWh for an anti-correlated pair to 4127 GWh for a well-correlated pair. Additionally, the well-correlated pair utilizes over 5 times as much storage, exhibits a 47% increase in average system cost, and an 69% increase in GHG emissions over the case of integrating two anti-correlated sites. On the other hand, increasing the number of wind regimes in a system

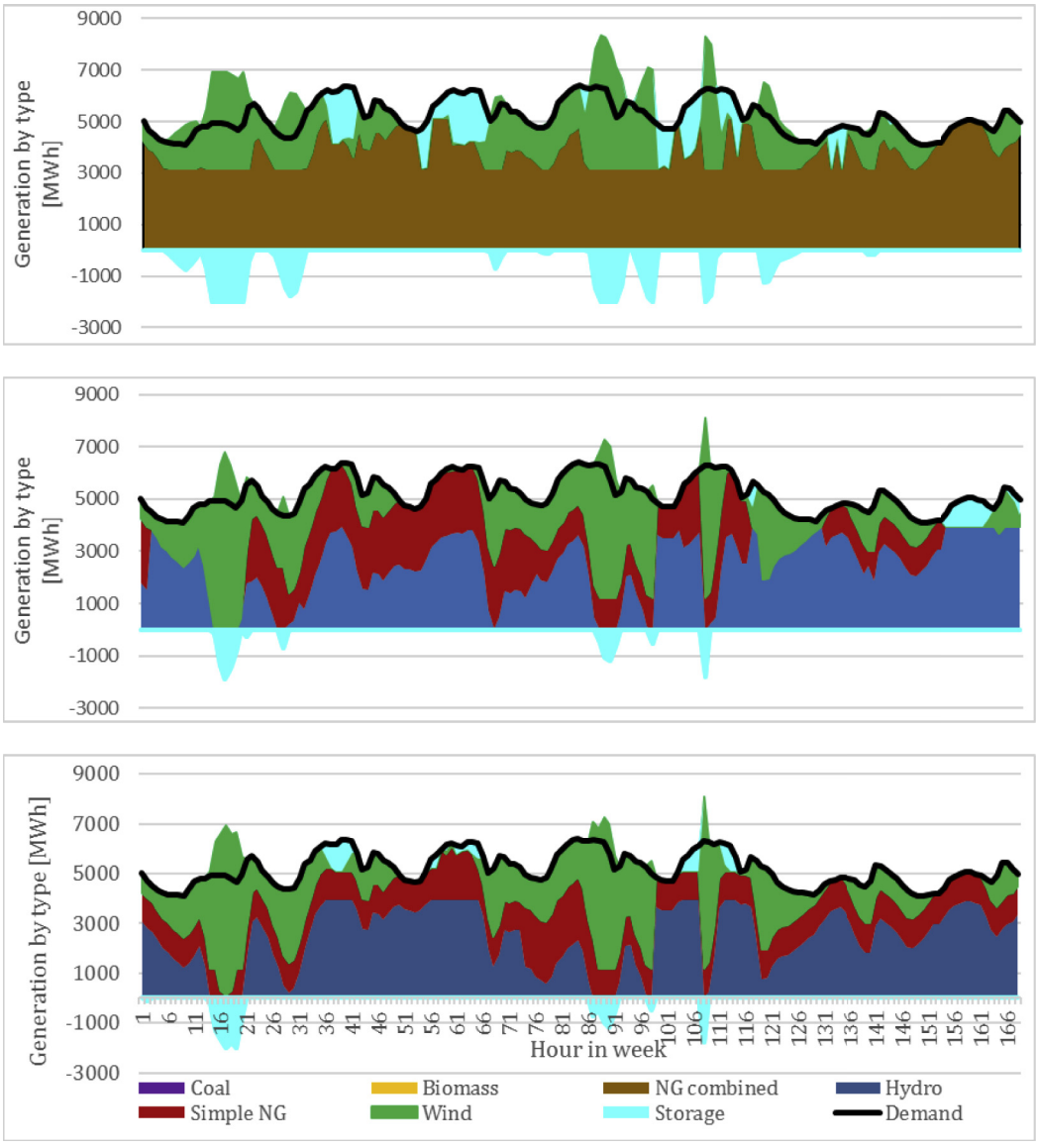

Fig. 21. Generation by technology type for a system with a low (top), average (middle), and high (bottom) flexibility factor, when integrating a variable wind resource.

has a much smaller impact on integration requirements as compared to integrating anti-correlated sets of wind regimes).

4.5. The impact of inter-resource correlation factor on integration requirements

Analogous to deploying two complementary wind regimes, deploying complementary wind and solar regimes results in smaller extreme negative or positive net loads, as shown in Fig. 28.

The larger negative net loads in the well-correlated set require more storage deployment to offset the curtailment that would otherwise occur. The well-correlated wind and solar set incurs almost 180% more wind curtailment, over 800% more solar curtailment, and 50% more storage utilization as compared to the scenario integrating two anti-correlated sets. An example week

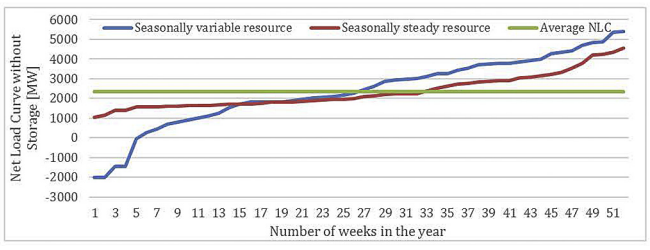

Fig. 22. Net load curve of a seasonally variable and steady resource without storage assets.

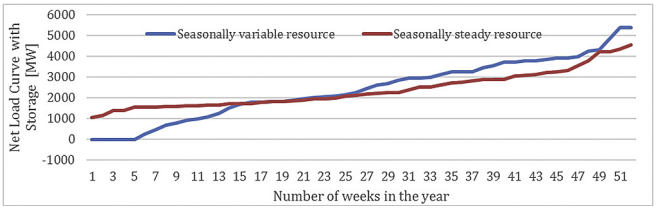

Fig. 23. Net load curve of a seasonally variable and steady resource with storage utilization.

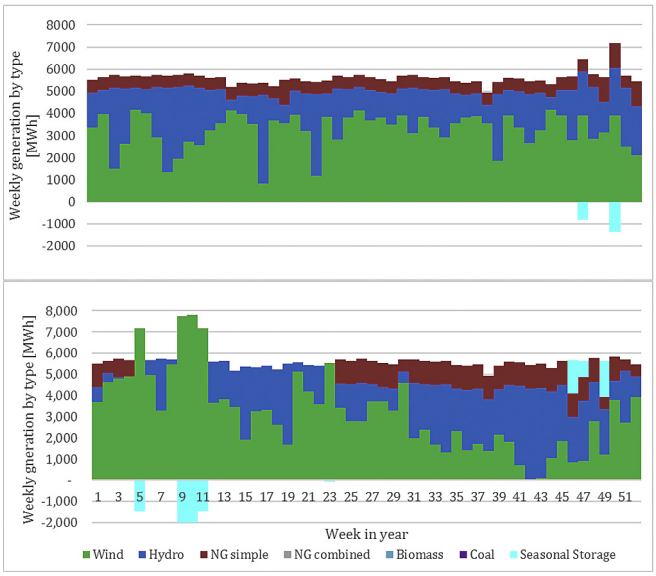

Fig. 24. Generation by technologies type in a system integrating a seasonally steady resource (top) versus a seasonally variable resource (bottom).

demonstrating the difference between integrating a well-correlated and anti-correlated wind-solar pair is shown in Fig. 29.

Additionally, integrating a well-correlated wind and solar regime incurs a 20% increase in average cost, 37% increase in marginal cost variability, 15% increase in GHG emissions, and 19% increase in non-VRE ramping events.

5. Discussion

5.1. Relative impact of alternative integration strategies

The overall impact associated with integrating VRE regimes on the grid differs depending on the integration scenario. Decreasing the system's non-VRE flexibility factor increases the cumulative integration costs most significantly, as measured by average marginal cost (100%), GHG emissions (100%), VRE curtailment (100%), and storage and DR asset utilization (90%). Integrating a regime that is anti-correlated with the demand profile, charging curtailment costs, and integrating a highly variable VRE regime, also increase integration costs, but to a lesser extent. On the other hand, integrating an anti-correlated pair of wind regimes incurs the least integration requirements, as measured by average marginal cost (almost 40% of relative impact), GHG emissions (20%), VRE curtailment (<0.05%), and storage and DR utilization (3%). In terms of VRE integration requirements, this scenario is followed by integrating an anti-correlated wind and solar pair. Deploying two anti-correlated wind pairs is a better strategy than deploying an anti-correlated wind-solar pair. The most effective balancing strategy that does not require multi-project coordination is to deploy VRE resources with low hourly variability. The relative impact of VRE variability on different integration metrics is summarized in Fig. 30.

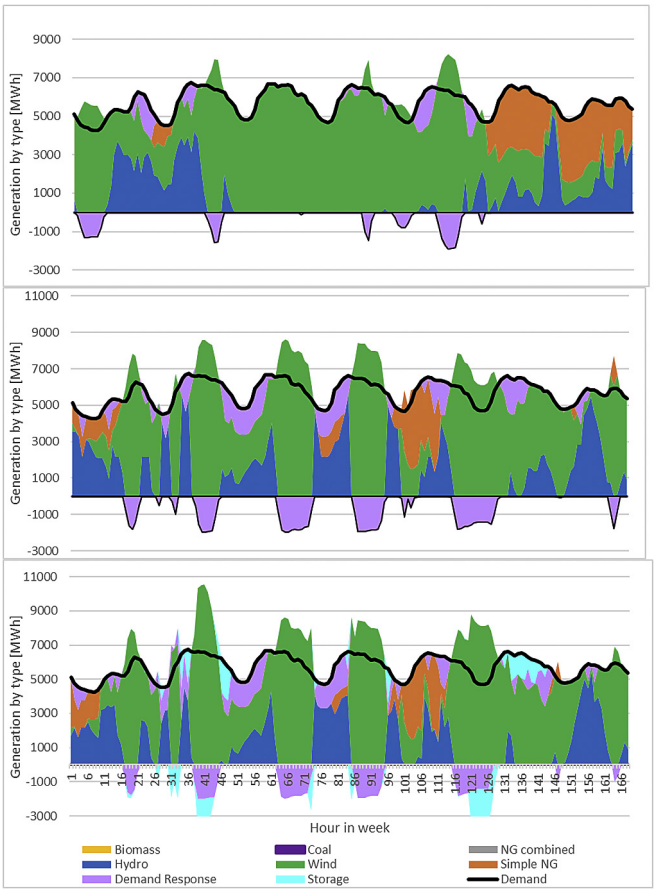

Fig. 26. Generation by technology type for an example week integrating a wind resource that is well-correlated with the demand profile (top), anti-correlated with the demand profile (middle), and anti-correlated with demand but includes both demand response and storage (bottom).

The results from this analysis contribute to the growing discussion on the impacts of VRE integration. Denholm and Hand provided one of the early VRE integration impact assessments by quantifying the curtailment and relative VRE costs of electricity systems with increasing VRE penetrations [13]. They highlight the significant impact of the system's flexibility factor on VRE integration metrics [13], which is a key factor in this analysis as well. More specifically, Denholm and Hand find that achieving 80% VRE penetration necessitates eliminating baseload "must-run" generation and addressing the mismatch between VRE supply and

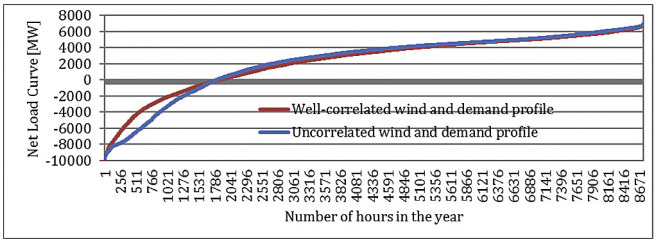

Fig. 25. Net load curve for a wind regime that is well-correlated with the demand profile versus a wind regime that is anti-correlated with the demand profile.

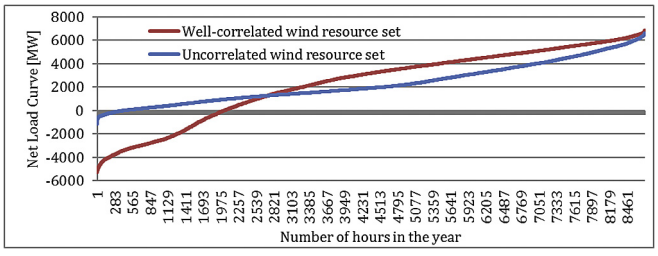

Fig. 27. Net load curve of two well-correlated and anti-correlated wind regimes.

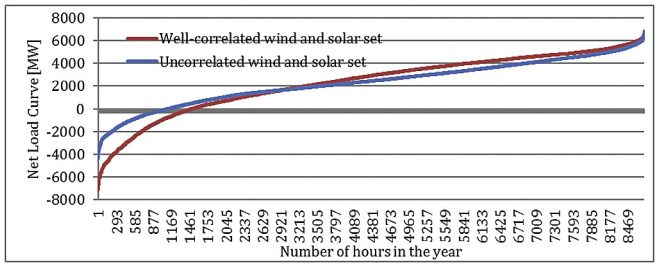

Fig. 28. Net load curve of a well-correlated wind and solar regime versus an anti-correlated wind and solar regime.

electricity demand [13]. Additionally, Frew et al. determine the impacts of integrating four flexibility mechanisms in high VRE penetration scenarios: geographic aggregation, renewable over-generation, storage, and flexible load [15]. From a cost perspective, Frew et al. find that geographic aggregation has the greatest system benefit [15]. Like Denholm and Hand, Frew et al. highlight the need for flexible load as VRE penetration increases to increase asset utilization rates and decrease system levelized costs [15]. Kondziella and Bruckner synthesize recent analyses of flexibility requirements for high-VRE penetration [25]. Their results show the wide range for flexibility demand at differing VRE penetrations; for example at 80% VRE penetration, demand for flexibility ranges from 40 to 120 GW for the German power sector [25]. This wide range reflects the range of assumptions that impact VRE integration metrics. Analyses of VRE integration in South America are less common. Schmidt et al. optimize the portfolio of hydro, wind and solar PV in Brazil to minimize thermal power production and its associated GHG emissions [43]. Using a daily dispatch model Schmidt et al. find that existing hydropower capacity can balance the variability from a 46% penetration of renewable electricity, assuming access to 24 h of electricity storage, adequate transmission expansions, and land availability [43]. The analysis in the present paper contributes to this VRE integration discussion, through a greater understanding of the implications of distinct VRE resource typologies. By developing VRE characterization metrics in the context of integration analyses, the current analysis provides a new perspective on VRE integration impact analysis which could improve electricity system planning activities.

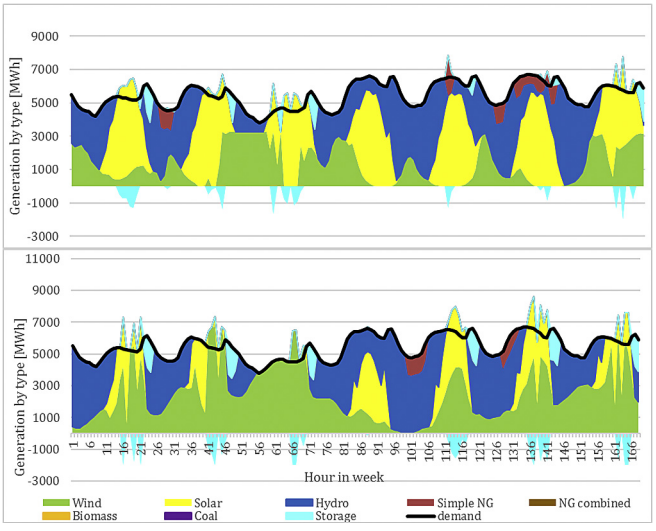

Fig. 29. Generation by technology type for an anti-correlated (top) versus a well-correlated (bottom) wind and solar pair.

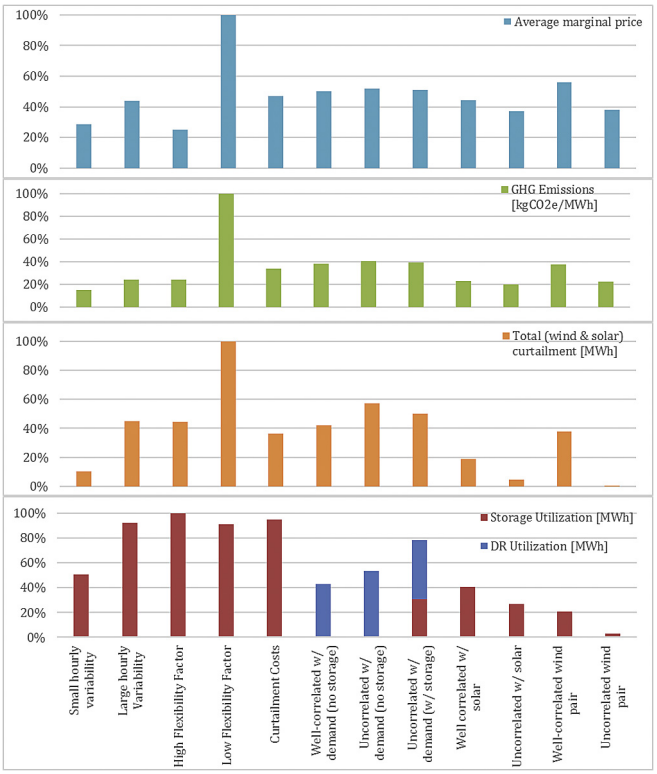

Fig. 30. Relative impact of VRE variability on different integration strategies (hourly scale).

5.2. Limitations of the analysis

This analysis embodies numerous approximations and assumptions. There are limitations in the MERRA dataset itself: the assimilation data are imperfect, the large spatial resolution of data masks local variations in resource quality, and the hourly temporal resolution occludes sub-hourly variability; variability at the millisecond, second, and minutes scale has been analyzed by Refs. [30,36,45]. The methodology used to select specific wind and solar grid points is simplistic, only considering the average resource value, and thus ignoring important factors such as proximity to transmission infrastructure, construction suitability, or access to transport networks. Additionally, the VRE power models inevitably embody sources of error. The variability metrics entail limitations associated with their highly aggregated formulations. While this aggregation enables visualization of overall trends, extreme but infrequent events are averaged out. Additionally, the block-form demand profile used for the DR metric includes historical data from only one South American electricity system (Chile), and remains constant throughout the 35-year analysis period. Finally, the UC model employs assumptions which may lack accuracy by assuming generalized generator characteristics. VRE regimes deployed in the UC were chosen to highlight the impact of different VRE characterizations, are not necessarily representative of 'realistic' VRE projects.

6. Conclusions

This paper proposes a methodology for characterizing variable renewable energy sources in terms of the balancing strategies that can be employed to integrate them into the existing electrical system. The methodology epitomizes the tradeoff between maximizing widespread relevancy, while maintaining sufficient

accuracy; the goal is to develop an integrated framework that can provide a suitable high level perspective for planners during a proposed electricity system transition. Variability on an hourly basis is quantified based on the frequency and magnitude of hourly ramp events, with relevance to flexibility resources with hourly dispatchability and reservoir size. Weekly-to-seasonal variability is characterized using relative frequency distributions. Inter-annual variability is quantified using the annual average resource over the 35-year period, informing long term backup or storage infrastructure requirements. The correlation between the VRE resource and the demand profile is quantified by calculating the average resource within distinct demand bands, informing the need for demand response initiatives. Analogously, the correlation between wind and solar resource is quantified to inform the value of interconnecting neighboring sites with transmission capacity. Finally, the geographic coincidence function for increasingly large geographic areas informs the value of expanding interconnections to increasingly large areas.

This characterization methodology is illustrated using South America and the results clearly identify the most prevalent VRE regimes. The results illustrate the relationships between different categories of balancing options. Approximately half of the wind grid points fit into one of nine types with varying degrees of requirements in each balancing category. The two most prevalent wind types are also the most demanding in terms of balancing requirements. Yet, significantly, as much as 10% of the South American wind regimes appear to need little investment in the form of balancing infrastructure.

System-level planning is the most important integration strategy. Strategic resource planning, by deploying anti-correlated wind-wind or wind-solar pairs, and strategic system planning, by designing high-flexibility-factor systems, are the two most effective strategies to mitigate VRE integration costs.

The goal of this characterization is to contribute to the set of tools that electricity system planners can leverage when planning high VRE penetrations. Local planners can apply these tools to quantify the requirements for balancing resources, given different combinations of wind and solar types.

Acknowledgements

We gratefully acknowledge Natural Sciences and Engineering Research Council of Canada (NSERC) and Hatch for their funding.

References

[1] M. Al-Nory, M. El-Beltagy, An energy management approach for renewable energy integration with power generation and water desalination, Renew. Energy 72 (Complete) (2014) 377–385, http://dx.doi.org/10.1016/j.renene.2014.07.032.
[2] C.L. Archer, M.Z. Jacobson, Spatial and temporal distributions of U.S. winds and wind power at 80 m derived from measurements, J. Geophys. Res. 108 (D9) (2003), http://dx.doi.org/10.1029/2002JD002076.
[4] Black & Vetch Holding Company, Cost and performance data for power generation technologies, National Renewable Energiy Laboratory, 2012.
[5] N. Boccard, Capacity factor of wind power realized values vs. estimates, Energy Policy 37 (7) (2009) 2679–2688, http://dx.doi.org/10.1016/j.enpol.2009.02.046.
[6] J. Boland, B. Ridley, B. Brown, Models of diffuse solar radiation, Renew. Energy 33 (4) (2008) 575–584, http://dx.doi.org/10.1016/j.renene.2007.04.012.
[7] M.C. Brower, M.S. Barton, L. Lledó, J. Dubois, A Study of Wind Speed Variability Using Global Reanalysis Data, 2013.
[8] B. Burgholzer, H. Auer, Cost/benefit analysis of transmission grid expansion to enable further integration of renewable electricity generation in Austria, Renew. Energy 97 (Complete) (2016) 189–196, http://dx.doi.org/10.1016/j.renene.2016.05.073.
[9] Central Energia, Central de información y discusión de energía en Chile, 2015. Retrieved January 15, 2015, from, http://www.centralenergia.cl/en/electricity-generation-chile/.
[10] Coordinador Electrico Nacional, Informes Y Documentos, 2015. Retrieved January 15, 2015, from, https://sic.coordinadorelectrico.cl/informes-y-documentos/.
[11] A. Cosseron, U.B. Gunturu, C.A. Schlosser, Characterization of the wind power resource in Europe and its intermittency, Energy Procedia 40 (2013) 58–66, http://dx.doi.org/10.1016/j.egypro.2013.08.008.
[12] J.P. Deane, Á. Driscoll, B.P.Ó. Gallachóir, Quantifying the impacts of national renewable electricity ambitions using a North–West European electricity market model, Renew. Energy 80 (Complete) (2015) 604–609, http://dx.doi.org/10.1016/j.renene.2015.02.048.
[13] P. Denholm, M. Hand, Grid flexibility and storage required to achieve very high penetration of variable renewable electricity, Energy Policy 39 (3) (2011) 1817–1830, http://dx.doi.org/10.1016/j.enpol.2011.01.019.
[14] C. Fant, U.B. Gunturu, Characterizing Wind Power Resource Reliability in Southern Africa, WIDER Working Paper, 2013.
[15] B.A. Frew, S. Becker, M.J. Dvorak, G.B. Andresen, M.Z. Jacobson, Flexibility mechanisms and pathways to a highly renewable US electricity future, Energy 101 (2016) 65–78, http://dx.doi.org/10.1016/j.energy.2016.01.079.
[16] P. Gilman, S. Cowlin, D. Heimiller, Potential for Development of Solar and Wind Resource in Bhutan, 2009. Retrieved from, http://www.nrel.gov/docs/fy09osti/46547.pdf.
[17] L. Göransson, F. Johnsson, Dispatch modeling of a regional power generation system – integrating wind power, Renew. Energy 34 (4) (2009) 1040–1049, http://dx.doi.org/10.1016/j.renene.2008.08.002.
[18] A. Greenhall, R. Christie, J.P. Watson, Minpower: a power systems optimization toolkit, in: IEEE Power and Energy Society General Meeting, 2012, http://dx.doi.org/10.1109/PESGM.2012.6344667.
[19] U.B. Gunturu, C.A. Schlosser, Characterization of wind power resource in the United States, Atmos. Chem. Phys. 12 (20) (2012) 9687–9702, http://dx.doi.org/10.5194/acp-12-9687-2012.
[20] W. Henson, J. McGowan, J. Manwell, Utilizing reanalysis and synthesis datasets in wind resource characterization for large-scale wind integration, Wind Eng. 36 (1) (2012) 97–110, http://dx.doi.org/10.1260/0309-524X.36.1.97.
[21] L. Hirth, F. Ueckerdt, O. Edenhofer, Integration costs revisited – an economic framework for wind and solar variability, Renew. Energy 74 (2015) 925–939, http://dx.doi.org/10.1016/j.renene.2014.08.065.
[22] H. Holttinen, J. Kiviluoma, A. Estanqueiro, T. Aigner, Y.-H. Wan, M. Milligan, Variability of Load and Net Load in Case of Large Scale Distributed Wind Power, 2010.
[23] O.A. Jaramillo, M.A. Borja, Wind speed analysis in La Ventosa, Mexico: a bimodal probability distribution case, Renew. Energy 29 (10) (2004) 1613–1630, http://dx.doi.org/10.1016/j.renene.2004.02.001.
[24] J.D. Kern, D. Patino-Echeverri, G.W. Characklis, An integrated reservoir-power system model for evaluating the impacts of wind integration on hydropower resources, Renew. Energy 71 (Complete) (2014) 553–562, http://dx.doi.org/10.1016/j.renene.2014.06.014.
[25] H. Kondziella, T. Bruckner, Flexibility requirements of renewable energy based electricity systems - a review of research results and methodologies, Renew. Sustain. Energy Rev. (2016), http://dx.doi.org/10.1016/j.rser.2015.07.199.
[26] R. Lucchesi, File Specification for MERRA Products, GMAO Office Note No. 1 (Version 2.3), Global Modelling and Assimilation Office: NASA, 2012. Retrieved from, http://gmao.gsfc.nasa.gov/pubs/office_notes.
[27] H. Lund, Large-scale integration of optimal combinations of PV, wind and wave power into the electricity supply, Renew. Energy 31 (4) (2006) 503–515, http://dx.doi.org/10.1016/j.renene.2005.04.008.
[28] X. Luo, J. Wang, M. Dooner, J. Clarke, Overview of current development in electrical energy storage technologies and the application potential in power system operation, Appl. Energy 137 (2014) 511–536, http://dx.doi.org/10.1016/j.apenergy.2014.09.081.
[29] J.D. Maddaloni, A.M. Rowe, G.C. van Kooten, Wind integration into various generation mixtures, Renew. Energy 34 (3) (2009) 807–814, http://dx.doi.org/10.1016/j.renene.2008.04.019.
[30] Y.V. Makarov, S. Member, C. Loutan, J. Ma, P. De Mello, S. Member, Operational impacts of wind generation on California power systems, IEEE Trans. Power Syst. 24 (2) (2009) 1039–1050.
[31] M. McPherson, T. Sotiropoulos-Michalakaos, D. Harvey, B. Karney, An Open-access Web-based Tool to Access Global, Hourly Wind and Solar PV Generation Time-series Derived from the MERRA Reanalysis Dataset, 2017. Submitted.
[32] I. Moazzen, B. Robertson, P. Wild, A. Rowe, B. Buckham, Impacts of large-scale wave integration into a transmission-constrained grid, Renew. Energy 88 (Complete) (2016) 408–417, http://dx.doi.org/10.1016/j.renene.2015.11.049.
[33] M.L. Morrissey, W.E. Cook, J.S. Greene, An improved method for estimating the wind power density distribution function, J. Atmos. Ocean. Technol. 27 (7) (2010) 1153–1164, http://dx.doi.org/10.1175/2010JTECHA1390.1.
[34] National Renewable Energy Laboratory (NREL), Dynamic Maps, GIS Data, and Analysis Tools - Wind Data Details, 2014. Retrieved March 1, 2014, from, http://www.nrel.gov/gis/wind_detail.html.
[35] J.V. Paatero, P.D. Lund, Effects of large-scale photovoltaic power integration on electricity distribution networks, Renew. Energy 32 (2) (2007) 216–234, http://dx.doi.org/10.1016/j.renene.2006.01.005.
[36] B.K. Parsons, M. Milligan, J.C. Smith, E. DeMeo, B. Oakleaf, K. Wolf, D.Y. Nakafuji…, Grid Impacts of Wind Power Variability: Recent Assessments from a Variety of Utilities in the United States, National Renewable Energy Laboratory, 2006.
[37] Parsons Brinckerhoff, Technical Assessment of the Operation of Coal and Gas

Fired Plants, 2014. West Yorkshire.
[38] R. Perez, R. Seals, P. Ineichen, R. Stewart, D. Menicucci, New simplified version of the Perez diffuse irradiance model for tilted surfaces, Sol. Energy 39 (3) (1987) 221–231.
[39] L. Ramirez Camargo, W. Dorner, Comparison of satellite imagery based data, reanalysis data and statistical methods for mapping global solar radiation in the Lerma Valley (Salta, Argentina), Renew. Energy 99 (2016) 57–68, http://dx.doi.org/10.1016/j.renene.2016.06.042.
[40] M.M. Rienecker, M.J. Suarez, R. Gelaro, R. Todling, J. Bacmeister, E. Liu, … J. Woollen, MERRA: NASA's modern-Era Retrospective analysis for research and applications, J. Clim. 24 (2011).
[41] W.-P. Schill, M. Pahle, C. Gambardella, On Start-up Costs of Thermal Power Plants in Markets with Increasing Shares of Fluctuating Renewables, 2016. Retrieved from, http://papers.ssrn.com/abstract=2723897.
[42] S. Schlomer, T. Bruckner, L. Fulton, E. Hertwich, A. McKinnon, D. Perczyk, … R. Wiser, Annex III: Technology-specific Cost and Performance Parameters, in: Climate Change 2014: Mitigation of Climate Change, 2014, pp. 1329–1356. Contribution of Working Group III to the Fifth Assessment Report of the Intergovernmental Panel on Climate Change.
[43] J. Schmidt, R. Cancella, A.O. Pereira Jr., An optimal mix of solar PV, wind and hydro power for a low-carbon electricity supply in Brazil, Renew. Energy 85 (2016) 137–147, http://dx.doi.org/10.1016/j.renene.2015.06.010.
[44] G.M. Shafiullah, Hybrid renewable energy integration (HREI) system for subtropical climate in Central Queensland, Australia, Renew. Energy 96 (Part A) (2016) 1034–1053, http://dx.doi.org/10.1016/j.renene.2016.04.101.
[45] J.C. Smith, M.R. Milligan, E.A. DeMeo, B. Parsons, Utility wind integration and operating impact state of the art, IEEE Trans. Power Syst. 22 (3) (2007) 900–908, http://dx.doi.org/10.1109/tpwrs.2007.901598.
[46] U.S. Energy Information Administration, Annual Energy Outlook 2014 Cost and Performance Characteristics of New Central Station Electricity Generating Technologies, 2014. Retrieved from, http://www.eia.gov/forecasts/aeo/assumptions/pdf/0554(2014).pdf.
[47] U.S. Energy Information Administration, Levelized Cost and Levelized Avoided Cost of New Generation Resources in the Annual Energy Outlook 2014, (March), 2014, pp. 1–12.
[48] H. Valizadeh Haghi, M. Tavakoli Bina, M.A. Golkar, S.M. Moghaddas-Tafreshi, Using Copulas for analysis of large datasets in renewable distributed generation: PV and wind power integration in Iran, Renew. Energy 35 (9) (2010) 1991–2000, http://dx.doi.org/10.1016/j.renene.2010.01.031.
[49] S. Weitemeyer, D. Kleinhans, T. Vogt, C. Agert, Integration of Renewable Energy Sources in future power systems: the role of storage, Renew. Energy 75 (Complete) (2015) 14–20, http://dx.doi.org/10.1016/j.renene.2014.09.028.
[50] E.I. Zoulias, N. Lymberopoulos, Techno-economic analysis of the integration of hydrogen energy technologies in renewable energy-based stand-alone power systems, Renew. Energy 32 (4) (2007) 680–696, http://dx.doi.org/10.1016/j.renene.2006.02.005.